Surface waves from flexural and compressional resonances of beams

Jean-Jacques Marigo, Kim Pham, Agnes Maurel, Sébastien Guenneau

Surface waves from flexural and compressional resonances of beams

Jean-Jacques Marigo
Lab. de Mécanique des Solides, Ecole Polytechnique, Route de Saclay, 91120 Palaiseau, France

Kim Pham
IMSIA, CNRS, EDF, CEA, ENSTA Paris, Institut Polytechnique de Paris, 828 Bd des Maréchaux, 91732 Palaiseau, France

Agnès Maurel
Institut Langevin, ESPCI ParisTech, CNRS, 1 rue Jussieu, 75005 Paris, France

Sébastien Guenneau
UMI 2004 Abraham de Moivre-CNRS, Imperial College, London SW7 2AZ, UK

We present a three-dimensional model describing the propagation of elastic waves in a soil substrate supporting an array of cylindrical beams experiencing flexural and compressional resonances. The resulting surface waves are of two types. In the sagittal plane, hybridized Rayleigh waves can propagate except within bandgaps resulting from a complex interplay between flexural and compressional resonances. We exhibit a wave decoupled from the hybridized Rayleigh wave which is the elastic analogue of electromagnetic spoof plasmon polaritons. This wave with displacements perpendicular to the sagittal plane is sensitive only to flexural resonances. Similar, yet quantitatively different, physics is demonstrated in a two-dimensional setting involving resonances of plates.

Surface elastic waves can propagate in a soil substrate supporting a periodic array of resonating elements. This has been chiefly demonstrated in the GHz regime with resonant pillars of typically 1/10 micrometer scale [1–4]. Considering meter length scale the frequency range falls in the spectrum of seismic waves and in this context, an array of beams on a soil substrate is the canonic idealized configuration used in seismology to illustrate the problem of "site-city interaction" [5]. From a theoretical point of view, most of the models encapsulate the behavior of the resonators with a single or multi-degree of freedom system, resulting in effective boundary conditions of the Robin type for the soil on its own [6–8]. On the basis of these models new devices of seismic metasurfaces have been shown to efficiently shield Rayleigh [9–14] and Love [15–17] waves. In most cases, only the compressional resonances of the resonators were considered. In a recent work, the case of flexural resonances of beams has been considered [18]. However, the study does not address the configuration of beams in perfect contact with the soil and merely considers motions in the sagittal plane due to flexural resonances.

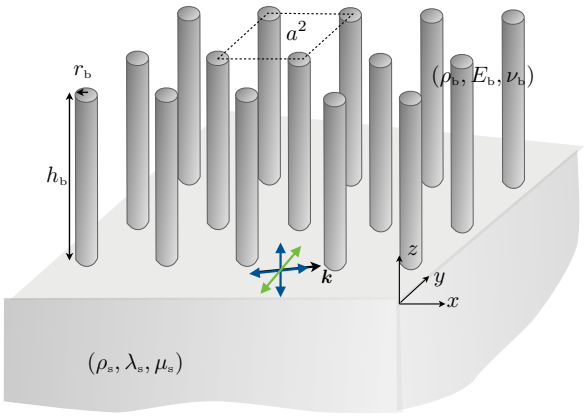

FIG. 1: Soil substrate supporting an array of beams with flexural and compressional resonances. Hybridized Rayleigh waves with motions in the sagittal plane (blue arrows show the displacements in the sagittal plan) and out-of-plane elastic SPPs (green arrows).

In this Letter we consider this realistic configuration and we propose a model able to account for both flexural and compressional resonances in three dimensions, see Figure 1. In the sagittal plane, hybridized Rayleigh waves are found whose dispersion results from a complex interplay between both types of resonances; in particular two Rayleigh waves can coexist at the same frequency. In addition, a surface wave with displacements perpendicular to the sagittal plane appears to be the elastic analog of spoof plasmon polaritons (SPPs) in electromagnetism [19] with a dispersion governed by the flexural resonances only. The two-dimensional case of an array of parallel plates can be modelled almost identically and unveils important quantitative differences with the three-dimensional case.

We denote $(\rho_\mathrm{b}, E_\mathrm{b}, \nu_\mathrm{b})$ the mass density, Young's modulus and the Poisson ratio of the beams; $(\rho_\mathrm{s}, \lambda_\mathrm{s}, \mu_\mathrm{s})$ are the mass density and the two Lamé's coefficients of the elastic soil substrate. When slender beams are considered, meaning that their radius r_b is much smaller than their height h_b, a reduction of model from three dimensions to one (vertical) dimension is possible and this results in

the well-known equations

$$\begin{cases} \dfrac{\partial^4 U_\alpha}{\partial z^4} - \kappa^4 U_\alpha = 0, \quad \alpha = x, y, \\ \dfrac{\partial^2 U_z}{\partial z^2} + K^2 U_z = 0, \end{cases} \tag{1}$$

where U_α, $\alpha = x, y$, are the horizontal displacements in the region of the beams and U_z the vertical displacement, see *e.g.* [13, 18]. In (1), the wavenumbers $\kappa = \left(\frac{4\rho_\mathrm{b}\omega^2}{E_\mathrm{b} r_\mathrm{b}^2}\right)^{1/4}$ and $K = \omega\sqrt{\frac{\rho_\mathrm{b}}{E_\mathrm{b}}}$ are associated with flexural and compressional resonances respectively. These equations have to be supplied with boundary conditions at the top of the beams and at their junction with the soil substrate. In the actual problem stress-free boundary condition apply at the top of the beams and the continuity of the displacements and of the normal stresses applies at the beam/soil interface. In the reduced model, this leads to clamped-free effective boundary conditions namely

$$\begin{cases} \text{at } z = 0: \ U_\alpha = u_\alpha, \quad \dfrac{\partial U_\alpha}{\partial z} = 0, \quad U_z = u_z, \\ \qquad\qquad \sigma_{z\alpha} = -\theta E_\mathrm{b} \dfrac{r_\mathrm{b}^2}{4} \dfrac{\partial^3 U_\alpha}{\partial z^3}, \quad \sigma_{zz} = \theta E_\mathrm{b} \dfrac{\partial U_z}{\partial z}, \\ \text{at } z = h_\mathrm{b} \quad \dfrac{\partial^2 U_\alpha}{\partial z^2} = \dfrac{\partial^3 U_\alpha}{\partial z^3} = 0, \quad \dfrac{\partial U_z}{\partial z} = 0, \end{cases} \tag{2}$$

where (u_α, u_z) are the displacements in the soil, $(\sigma_{z\alpha}, \sigma_{zz})$ the associated normal stress and θ the cross-sectional area ratio of beam or plate in the unit cell of horizontal extent a, see Table I. It is worth noting that such conditions can be either postulated as in [18] or derived using asymptotic analysis combined with homogenization [16, 17, 20].

The conditions of prescribed displacements and zero rotation at $z = 0$ together with the conditions of free rotation and free horizontal displacements at $z = h_\mathrm{b}$ make it possible to set the problem in the beams as two decoupled linear problems on U_α and U_z with respect to $u_{\alpha|z=0}$ and $u_{z|z=0}$ respectively. Denoting ω_0 the characteristic flexural frequency and ε the coupling parameter

$$\omega_0 = \frac{1}{\mathcal{S} h_\mathrm{b}} \sqrt{\frac{E_\mathrm{b}}{\rho_\mathrm{b}}}, \quad \varepsilon = \frac{\theta}{\mathcal{S}} \sqrt{\frac{\rho_\mathrm{b} E_\mathrm{b}}{\rho_\mathrm{S} \mu_\mathrm{S}}}, \tag{3}$$

where θ and $\mathcal{S}$ are given in table I (beams), we introduce the dimensionless frequency $\Omega = \omega/\omega_0 = (\kappa h_\mathrm{b})^2$.

	slenderness $\mathcal{S}$	filling fraction θ
3D (beams)	$\mathcal{S} = 2h_\mathrm{b}/r_\mathrm{b}$	$\theta = \pi r_\mathrm{b}^2/a^2$
2D (plates)	$\mathcal{S} = \sqrt{3(1-\nu_\mathrm{b}^2)} h_\mathrm{b}/r_\mathrm{b}$	$\theta = 2r_\mathrm{b}/a$

TABLE I: Slenderness $\mathcal{S}$ and filling fraction θ for beams and plates (with a the array spacing) entering in (3) resulting in the same modelling (4).

From (1)-(2), boundary conditions of the Robin's type are found for the substrate on its own

$$\begin{cases} \sigma_{x\alpha}(\boldsymbol{x}, 0) = \mu_\mathrm{S} k_\mathrm{T} \varepsilon \, f_\mathrm{F}(\Omega) \, u_\alpha(\boldsymbol{x}, 0), \quad \alpha = x, y \\ \sigma_{zz}(\boldsymbol{x}, 0) = \mu_\mathrm{S} k_\mathrm{T} \varepsilon \, f_\mathrm{C}(\Omega) \, u_z(\boldsymbol{x}, 0), \end{cases} \tag{4}$$

where $k_\mathrm{T} = \omega/c_\mathrm{T}$ ($c_\mathrm{T} = \sqrt{\mu_\mathrm{S}/\rho_\mathrm{S}}$) and

$$\begin{aligned} f_\mathrm{F}(\Omega) &= \sqrt{\Omega} \, \frac{\sin\sqrt{\Omega}\cosh\sqrt{\Omega} + \cos\sqrt{\Omega}\sinh\sqrt{\Omega}}{1 + \cosh\sqrt{\Omega}\cos\sqrt{\Omega}}, \\ f_\mathrm{C}(\Omega) &= \mathcal{S} \tan(\Omega/\mathcal{S}), \end{aligned} \tag{5}$$

being the impedance functions encapsulating the flexural and compressional resonances of the beams.

We are looking for a surface wave evanescent for $z \to -\infty$ and propagating along the interface $z = 0$ with a wavevector $\boldsymbol{k} = k\boldsymbol{n}$ ($\boldsymbol{n} = n_x \boldsymbol{e}_x + n_y \boldsymbol{e}_y$, $(\boldsymbol{e}_x, \boldsymbol{e}_y)$ being the unit vectors along x and y, and $n_x^2 + n_y^2 = 1$). The solution is written in terms of the elastic potentials $(\varphi, \boldsymbol{\psi})$, such that $\boldsymbol{u} = \Re[\boldsymbol{\nabla}\varphi + \boldsymbol{\nabla} \times \boldsymbol{\psi}]$, with $\boldsymbol{\nabla} \cdot \boldsymbol{\psi} = 0$. Making use of the isotropy of the medium, we define

$$\begin{cases} \varphi(\boldsymbol{x}, z) = -\dfrac{iA}{k} \, e^{k\alpha_\mathrm{L} z + i\boldsymbol{k}\cdot\boldsymbol{x}}, \\ \boldsymbol{\psi}(\boldsymbol{x}, z) = \dfrac{1}{k} \left(B_n \boldsymbol{n} + B_t \boldsymbol{t} + iB_z \boldsymbol{e}_z\right) e^{k\alpha_\mathrm{T} z + i\boldsymbol{k}\cdot\boldsymbol{x}}, \end{cases} \tag{6}$$

with $B_n + \alpha_\mathrm{T} B_z = 0$, and where $\boldsymbol{t} = -n_y \boldsymbol{e}_x + n_x \boldsymbol{e}_y$. With β the ratio of the celerities of the Rayleigh wave c and of the bulk shear wave c_T, we have

$$\beta = \frac{k_\mathrm{T}}{k}, \quad 1 - \alpha_\mathrm{T}^2 = \beta^2, \quad 1 - \alpha_\mathrm{L}^2 = \xi\beta^2, \tag{7}$$

where $\xi = \mu_\mathrm{S}/(\lambda_\mathrm{S} + 2\mu_\mathrm{S})$. The resulting expressions of (u_α, u_z), $(\sigma_{z\alpha}, \sigma_{zz})$ along with (4) provide two decoupled systems, on the displacements (u_n, u_z) (with $u_n = n_x u_x + n_y u_y$ and $\sigma_n = n_x \sigma_{xz} + n_y \sigma_{yz}$ the associated stress) and on the out-of-plane displacement $u_t = -n_y u_x + n_x u_y$ and $\sigma_t = -n_y \sigma_{xz} + n_x \sigma_{yz}$ the associated stress. The displacements (u_n, u_z) in the sagittal plane correspond to hybridized Rayleigh waves whose dispersion relation reads

$$\begin{cases} \left(1 + \alpha_\mathrm{T}^2\right)^2 - 4\alpha_\mathrm{T}\alpha_\mathrm{L} + C_\varepsilon(\beta, \Omega) = 0, \\ C_\varepsilon(\beta, \Omega) = \ \varepsilon\beta^3 \left[f_\mathrm{C}\alpha_\mathrm{L} + f_\mathrm{F}\alpha_\mathrm{T}\right] + \varepsilon^2\beta^2 f_\mathrm{C} f_\mathrm{F} \left(\alpha_\mathrm{L}\alpha_\mathrm{T} - 1\right). \end{cases} \tag{8}$$

(where f stands for $f(\Omega)$). The displacement u_t perpendicular to the sagittal plane is associated with a surface wave whose dispersion

$$\beta = \frac{1}{\sqrt{1 + \varepsilon^2 f_\mathrm{F}^2(\Omega)}}, \quad f_\mathrm{F}(\Omega) \geq 0, \tag{9}$$

is the elastic analog of electromagnetic spoof plasmons [19]. Interestingly, such a wave has been announced in

a similar setting involving Love waves in the presence of a guiding layer (see Fig. 11 in [16]). As one would expect for $\varepsilon = 0$, the classical Rayleigh waves is recovered, see (8), and the elastic SPP disappears, see (9) (with $k = k_{\rm T}$). Next, neglecting the flexural resonances ($f_{\rm F} = 0$) produces $C_\varepsilon = \varepsilon\beta^3\alpha_{\rm L} f_{\rm C}$ in agreement with [13]. Eventually, considering the flexural resonances in a frequency range well below the first longitudinal resonance gives $f_{\rm C}(\Omega) \sim \Omega$ in agreement with [20].

From now on, we set the physical parameters as follows: $E_{\rm S} = 0.1$ GPa, $\rho_{\rm S} = 10^3$ kg.m^{-3} and $E_{\rm b} = 10E_{\rm S}$, $\rho_{\rm b} = 10\rho_{\rm S}$; $\nu_{\rm S} = \nu_{\rm b} = 0.3$ (hence $\xi \simeq 0.28$). Next, $r_{\rm b} = 0.25$ m and $a = 1$ m and we consider $h_{\rm b} = 30$, 15 and 6 m. The resulting parameters entering in (3) and (4) are given in Table II according to Table I.

	$h_{\rm b} = 30$ m	15 m	6 m
3D	$\omega_0 = 0.04$ rad.s^{-1} $\varepsilon = 1.3\,10^{-2}$ $\mathcal{S} = 240$	$\omega_0 = 0.17$ rad.s^{-1} $\varepsilon = 2.6\,10^{-2}$ $\mathcal{S} = 120$	$\omega_0 = 1.1$ rad.s^{-1} $\varepsilon = 6.6\,10^{-2}$ $\mathcal{S} = 48$
2D	$\omega_0 = 0.05$ rad.s^{-1} $\varepsilon = 3.8\,10^{-2}$ $\mathcal{S} = 210$	$\omega_0 = 0.21$ rad.s^{-1} $\varepsilon = 8.1\,10^{-2}$ $\mathcal{S} = 102$	$\omega_0 = 1.33$ rad.s^{-1} $\varepsilon = 20.3\,10^{-2}$ $\mathcal{S} = 40$

TABLE II: Reference frequency ω_0 ($\Omega = \omega/\omega_0$) and dimensionless coupling parameter ε and slenderness $\mathcal{S}$ entering in (4)-(5) for beams (3D) and plates (2D), see Table I.

We report in figure 2 the dispersion relations $\beta(\Omega)$ of the hybridized Rayleigh waves (blue lines) for decreasing beam heights $h_{\rm b}$ while keeping constant the range $\Omega \in (0, 200)$. This allows to keep the first 6 flexural resonances at constant values $\Omega = 3.5$, 22.0, 61.8, 75.3, 120.9 and 199.8 corresponding to $(1 + \cos\sqrt{\Omega}\cosh\sqrt{\Omega}) = 0$. Within this interval, the dimensionless compressional frequencies $\Omega_{\rm C} = \frac{(2n+1)\pi}{2}\mathcal{S}$, $n = 0, 1, \cdots$, decrease linearly with $h_{\rm b}$ while their frequencies $\omega_{\rm C} = \sqrt{\frac{E_{\rm b}}{\rho_{\rm b}}}\frac{(2n+1)\pi}{2h_{\rm b}}$ increase (but more slowly than the flexural resonance frequencies). For a large slenderness $h_{\rm b} = 30$ m, the first longitudinal resonance is sent to $\Omega \simeq 377$ ($\omega_{\rm C} = 16.5$ Hz) hence $f_{\rm C}(\Omega) \simeq \Omega$ in (8). In this case, it is easy to see that the $(n+1)^{\rm th}$ branch , $n = 1, \cdots$, of hybridized Rayleigh wave appears (for $\beta = 1$) before the $n^{\rm th}$ branch has reached its asymptote (for $\beta = 0$). The salient consequence is that the branches n and $(n+1)$ coexist below the $n^{\rm th}$ flexural resonance frequency. Decreasing the slenderness with $h_{\rm b} = 15$ m and 6 m leads to the appearance of the first compressional resonance frequency at $\Omega_{\rm C} = 188.5$ ($\omega_{\rm C} = 33.1$ Hz) and $\Omega_{\rm C} = 75.4$ ($\omega_{\rm C} = 82.8$ Hz). In these cases, relatively small bandgaps (light blue regions) are opened within the large bandgap dictated by the compressional resonance on its own (light red regions), revealing the interplay between the two types of resonances. Incidentally, as it is the rule, these intrinsic bandgaps (independent of the array spacing a) can

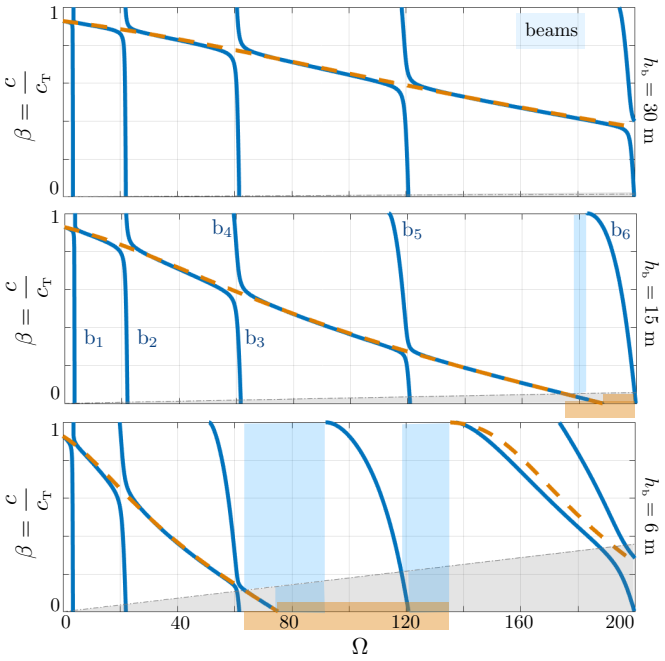

FIG. 2: Dispersion of the hybridized Rayleigh wave for 3D beams – dimensionless velocity $c/c_{\rm T}$ versus $\Omega = \omega/\omega_0$ (blue lines). Dashed red lines show the dispersion produced by the compressional resonances on their own ($f_{\rm F} = 0$). For $h_{\rm b} = 30$ m, there is no bandgap and two branches b$_n$ and b$_{n+1}$ coexist in a frequency range just below the $n^{\rm th}$ flexural resonance. For $h_{\rm b} = 15$ m a bandgap is opened by periodicity (light blue region in the Brillouin zone) and at $h_{\rm b} = 6$ m the two intrinsic bandgaps (light blue region outside of the Brillouin zone, independent of a) are slightly enlarged by periodicity.

be enlarged by periodicity which imposes $\beta \geq \left(\frac{\omega_0 a}{\pi c_{\rm T}}\right)\Omega$ ($k < \pi/a$) as seen for $h_{\rm b} = 6$ m; also, bandgaps solely due to periodicity can be opened as can be seen for $h_{\rm b} = 15$ m near $\Omega = 180$. Eventually, in figure 3 we report the dispersion relation of the elastic SPPs, from (9), for $h_{\rm b} = 6$ m. As their electromagnetic counterparts, these waves have bandgaps dictated by the condition $f_{\rm F} \geq 0$ hence the bandgap positions and thicknesses are independent of the coupling ε and of the slenderness $\mathcal{S}$. As previously

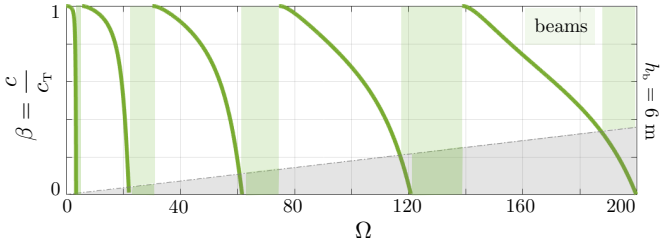

FIG. 3: Dispersion of elastic SPPs, from (9) with out-of-plane motion for $h_{\rm b} = 6$ m. Intrinsic band-gaps are opened due to flexural resonances (light green regions outside of the Brillouin zone) which are enlarged by periodicity (light green regions inside the Brillouin zone).

said, similar waves with out-of-plane displacements have been reported in the presence of a guiding layer [16], and they are recovered here in the absence of any guiding layer.

We now restrict ourselves on to a two-dimensional setting involving arrays of plates. As one would expect, the coupling of plates with the soil is higher than that of beams for the same thickness $2r_\mathrm{b}$ and the same height h_b (see table II); the slenderness $\mathcal{S}$ on the contrary is slightly lower which is also expected since plates have a higher flexural rigidity than beams, and this is translated in an effective lower slenderness, see table I. Accordingly, the relative positions of the compressional and flexural resonances change and we shall see that this strongly affects the dispersion of the hybridized Rayleigh waves. We provide in this case a numerical validation of the dispersion curves by means of diverging reflection coefficients computed below the sound line $k < k_\mathrm{T}$ using a multimodal method [21]. Results are shown in figure 4. The overall agreement is good for $h_\mathrm{b} = 30$ and 15 m although the condition of zero group velocity at the boundary of the Brillouin zone (vertical slope $\frac{\partial\beta}{\partial\Omega} = \infty$) produces more or less pronounced shifts of the branches to lower frequencies [22]. For $h_\mathrm{b} = 6$ m, the agreement is good up to $\Omega \sim 50$ which can be partially attributed to other resonances and in particular that of an edge mode for

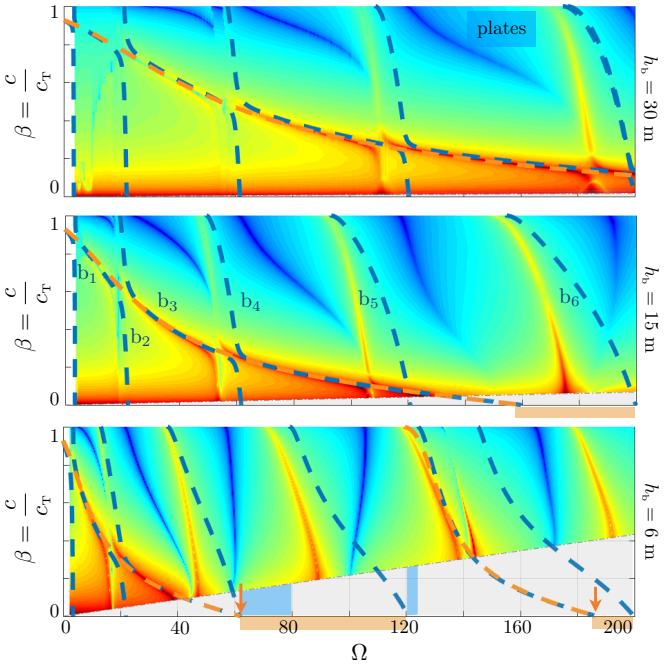

FIG. 4: Dispersion of the hybridized Rayleigh wave for 2D plates – The dispersion relations are obtained numerically in the actual problems by means of the divergence of the reflection coefficient (in logarithmic color scale with maxima in red, arbitrary scales have been used). Dashed blue lines show the dispersion from (8), red vertical arrows for $h_\mathrm{b} = 15$ m and 6 m indicate the occurence of compressional resonances.

$\sqrt{\frac{\rho_\mathrm{b}}{E_\mathrm{b}}}\omega h_\mathrm{b} \simeq 2.32$ ($\Omega = 91$) [23].

The ellipticity χ of surface waves of the Rayleigh type (or H/V for horizontal to vertical ratio) characterizes the displacements at the soil surface, namely $\chi = a/b$ for displacement at $z = 0$ of the form $u_n = a\cos(\boldsymbol{k}\cdot\boldsymbol{x} - \omega t)$, $u_z = b\sin(\boldsymbol{k}\cdot\boldsymbol{x} - \omega t)$ and it is an important indicator of the ground motion. From (8), it reads

$$\chi = \frac{\alpha_\mathrm{T}\beta^2 + \varepsilon\beta f_\mathrm{C}(\alpha_\mathrm{L}\alpha_\mathrm{T} - 1)}{2\alpha_\mathrm{L}\alpha_\mathrm{T} - (1+\alpha_\mathrm{T}^2)} = \frac{2\alpha_\mathrm{L}\alpha_\mathrm{T} - (1+\alpha_\mathrm{T}^2)}{\beta^2\alpha_\mathrm{L} + \varepsilon\beta f_\mathrm{F}(\alpha_\mathrm{L}\alpha_\mathrm{T} - 1)}, \tag{10}$$

whose variations versus Ω are reported in figure 5 for $h_\mathrm{b} = 15$ m (in the case of beams and plates). In the reported cases, the branches b_n, $n = 1$ to 5, are below the first compressional resonance. Making use of (10) along with (8), these branches have 3 typical points: (i) the starting point ($\beta = 1$) for which $\chi = \varepsilon f_\mathrm{C}$ which increases when $n = 1, \cdots, 5$ increases as f_C does; (ii) the frequency at which the wave motion transitions from prograde to retrograde with $\chi = 0$ when $f_\mathrm{F} \to \infty$ and this is consistent with (4) which predicts $u_n = 0$ at the flexural resonances, (iii) the ending point for $\beta \to 0$ resulting in $\chi = -1/\xi$ for any branch. Next the branch b_6 appears just before the longitudinal resonance where $f_\mathrm{C} \to \infty$ imposes $u_z = 0$. It results high values of χ in the neighborhood of the singularity and it is worth noting that this affects a branch which is dictated by the interplay of flexural and compressional resonances (this branch is missed if flexural motions are disregarded). For comparison, we have computed numerically the displacements at

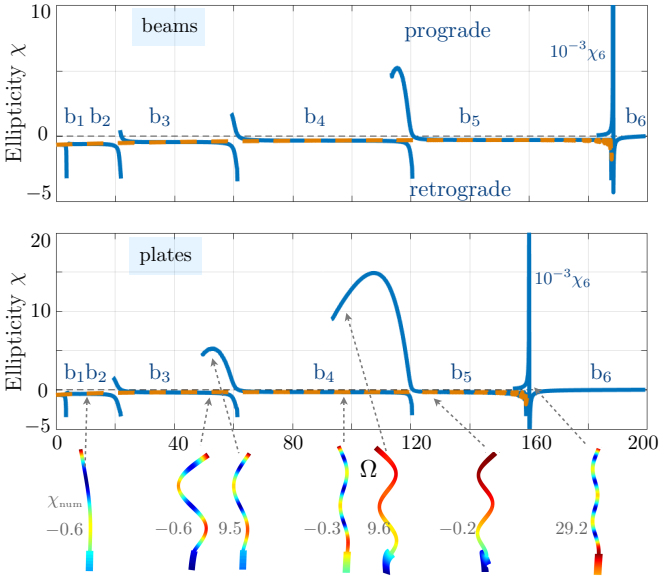

FIG. 5: Ellipticity χ of the hybridized Rayleigh waves versus Ω for beams (upper panel) and for plates – Blue lines show χ from (10), dashed red lines neglecting the flexion ($f_\mathrm{F} = 0$ in (10)). Insets show the deformations in the plates atop the soil in a single cell, computed numerically and the corresponding ellipticity χ_num (see main text).

the free surface and in the plates for $\Omega = 13$ (b_2), $\Omega = 50$ (coexistence of b_3 and b_4), $\Omega = 94$ (coexistence of b_4 and b_5), $\Omega = 122$ (b_5) and $\Omega = 156$ (b_6). Results, in the insets of figure 5, show the deformations in the plates and the corresponding ellipticity χ_{num}. The agreement with (10) is qualitative which is partly attributable to the existence of boundary layers at the junction between the plates and the soil. However they confirm the main trends of the model, in particular it is noticeable that the motions in the plates are dominantly horizontal even for very low ellipticity.

Beams and plates atop a soil substrate impact propagation of seismic waves in a richer way than their acoustic counterparts. This is due to a complex interplay between the compressional and longitudinal resonances and to their associated spectra. In particular, (i) the dispersion of hybridized Rayleigh waves shows a important part of the spectrum associated with celerities larger than that of the classical Rayleigh waves; (ii) These waves are associated with prograde or retrograde motion at the soil interface with large variations of the ellipticity; (iii) The existence of an out-of-plane surface wave, with infinite ellipticity on its own, sheds new light on the analysis of the displacement components in particular on records of the ambient noise for which the horizontal displacement is the sum of the two contributions [24, 25].

[1] A. Khelif, Y. Achaoui, S. Benchabane, V. Laude and B. Aoubiza, Phys. Rev. B **81**(21), 214303 (2010).
[2] Y. Achaoui, A. Khelif, S. Benchabane , L. Robert, and V. Laude, Phys. Rev. B **83**(10), 104201 (2011).
[3] M. Oudich, and M.B. Assouar, J. Appl. Phys. **111**(1), 014504 (2012).
[4] Y. Achaoui, V. Laude, S. Benchabane, and A. Khelif, J. Appl. Phys. **114**(10), 104503 (2013).
[5] P. Guéguen, P.Y. Bard, and J.F. Semblat, Proc. 12th World Conference on Earthquake Engineering. https://www.iitk.ac.in/nicee/wcee/article/0555.pdf (2000).
[6] E. Garova, A. Maradudin, and A. Mayer, Phys. Rev. B **59**(20) 13291 (1999).
[7] A. Maznev, and V. Gusev, Phys. Rev. B **92**(11) 115422 (2015).
[8] L. Schwan, and C. Boutin, Wave Motion **50**(4) 852-868 (2013).
[9] S. Brûlé, E. Javelaud, S. Enoch, and S. Guenneau, Phys. Rev. Lett. **112**(13) 133901 (2014).
[10] S. Krödel, N. Thomé, and C. Daraio, Ext. Mech. Lett. **4**(2015) 111-117 (2015).
[11] A. Colombi, P. Roux, S. Guenneau, P. Gueguen, and R.V. Craster, Scientific Rep. **6** 19238 (2016).
[12] A. Colombi, D. Colquitt, P. Roux, S. Guenneau, and R.V. Craster, Scientific Rep. **6**, 27717 (2016).
[13] D. Colquitt D, A. Colombi, R.V. Craster, P. Roux, and S. Guenneau, JMPS **99** 379-393 (2017).
[14] A. Palermo, S. Krödel, A. Marzani, and C. Daraio, Scientific Rep. **6** 39356 (2016).
[15] A. Palermo, and A. Marzani, Scientific Rep. **8**(1) 7234 (2018).
[16] A. Maurel, J.J. Marigo, K. Pham, and S. Guenneau, Phys. Rev. B **98**(13) 134311 (2018).
[17] K. Pham, A. Maurel, S. Félix, and S. Guenneau, Materials **13**(1), in press (2020).
[18] P.T. Wootton, J. Kaplunov, and D.J. Colquitt, Proc. R. Soc. A **475** 20190079 (2019).
[19] J.B. Pendry, L. Martin-Moreno, and F. Garcia-Vidal, Science **305** 847-848 (2004).
[20] J.J Marigo, K. Pham, A. Maurel, and S. Guenneau, submitted **Seb: (Arxiv)**
[21] A. Maurel, and K. Pham, J. Acoust. Soc. Am. **146**(6), 4402-4412 (2019).
[22] J.F. Mercier, M.L. Cordero, S. Félix, A. Ourir, and A. Maurel, Proc. R. Soc. A **471**(2182), 20150472 (2015).
[23] V. Pagneux, J. Acoust. Soc. Am. **120**(2), 649-656 (2006).
[24] E.F. Manea, C. Michel, M. Hobiger, D. Fäh, C.O. Cioflan, and M. Radulian, Geophys. J. Int. **210**(3), 1609-1622 (2017).
[25] M. Lott, P. Roux, S. Garambois, P. Guéguen, and A. Colombi, Geophys. J. Int. **220**(2), 1330-1339 (2019).